Performance analysis of hybrid system of multi effect distillation and reverse osmosis for seawater desalination via modeling and simulation

G. Filippini [1], M. A. Al-Obaidi [2, 3], F. Manenti [1], and I. M. Mujtaba [2, *]

[1] Chemical Engineering Department, School of Engineering, Faculty of Industrial Engineering, Politecnico di Milano, Milan, Piazza Leonardo da Vinci 32, Italy
[2] Chemical Engineering Division, Faculty of Engineering and Informatics, University of Bradford, Bradford, West Yorkshire BD7 1DP, UK
[3] Middle Technical University, Iraq – Baghdad
*Corresponding author, Tel.: +44 0 1274 233645
E-mail address: I.M.Mujtaba@bradford.ac.uk

Abstract

The coupling of thermal (Multi Stage Flash, MSF) and membrane processes (Reverse Osmosis, RO) in desalination systems has been widely presented in the literature to achieve an improvement of performance compared to an individual process. However, very little study has been made to the combined Multi Effect Distillation (MED) and Reverse Osmosis (RO) processes. Therefore, this research investigates several design options of MED with thermal vapor compression (MED_TVC) coupled with RO system. To achieve this aim, detailed mathematical models for the two processes are developed, which are independently validated against the literature. Then, the integrated model is used to investigate the performance of several configurations of the MED_TVC and RO processes in the hybrid system. The performance indicators include the fresh water productivity, energy consumption, fresh water purity, and recovery ratio. Basically, the sensitivity analysis for each configuration is conducted with respect to seawater conditions and steam supply variation. Most importantly, placing the RO membrane process upstream in the hybrid system generates the overall best configuration in terms of the quantity and quality of fresh water produced. This is attributed to acquiring the best recovery ratio and lower energy consumption over a wide range of seawater salinity.

Keywords**:** Seawater desalination, MED_TVC+RO hybrid system, Mathematical modeling, Sensitivity analysis.

1. Introduction

In the recent past, the demand for fresh water increased in many regions, especially in the developing countries, which in turn pushed the researchers toward more energy-efficient ways for seawater desalination. Coupling a power plant with a thermal desalination process allows to reach a greater thermal efficiency. This is attributed to the thermal energy produced from the power plant that would be used in the desalination process aside from wasting it. In this respect, the MSF was considered as the preferred technology to couple with a power plant. However, the low-temperature MED process proved to be more appropriate to couple with a power plant steam generator. This is due to employing low temperature steam in the MED process (Mahbub et al., 2009).

Over the last decades, the use of RO process as a complementary option with MED process is progressively increased. Interestingly, this technique acts in accordance with lower energy consumption with attaining the regulated limits of potable water issued by the World Health Organization (WHO, 2011). For instance, the Fujairah 2 desalination plant in the United Arab Emirates is one of the biggest desalination facilities in the world, with a capacity of 591000 m^3/day. Quantitatively, this facility consists of a 2000 MW power plant coupled with a 450000 m^3/day MED plant and a 136000 m^3/day RO plant (Veolia Water, 2011).

The desalination industry was growing very rapidly in the 2000s, and many researchers focused on the development of more efficient desalination processes, including hybrid systems. The next section illustrates several examples of the published research in the open literature regarding the hybrid systems of MED, with or without the thermal vapor compression (TVC) section, coupled with RO process.

Hamed (2005) reviewed the major features of commercially available hybrid desalination plants. The study confirmed that Nanofiltration (NF) membranes can be the best technology to couple with a thermal process, regarding fresh water productivity. Also, the full integration of membrane and thermal desalination processes provided a higher thermal performance than the simple integration. An economical evaluation of a small 2000 m^3/day MED+RO system powered by natural gas and includes heat recovery is carried out by Cardona et al. (2007). This in turn affirmed that the hybrid process can be more economical, producing fresh water with a lower specific cost per cubic meter. In the same context, Rensonnet et al. (2007) showed that the full hybridization of MED and RO is the most economical option if the electricity cost is high, otherwise the standalone RO process can be more convenient. Mahbub et al. (2009) proposed a detailed thermodynamic analysis of a combined cycle power (CCP) plant with MSF, MED and RO (standalone), or with hybrid MSF+RO and MED+RO. It is concluded that the specific energy consumption can be reduced by 17% with the CCP+MED+RO system, compared to CCP+MSF+RO system. Furthermore, the lowest cost of fresh water produced with the CCP+MED+RO option of about 1.09 $\$/m^3$.

The techno-economic performance of an integrated system of concentrating solar plant (CSP) with MED and Ultrafiltration (UF) is investigated by Olwig at al. (2012). The results showed the necessity of the RO process to improve the economics of the integrated process compared to a simple CSP+MED configuration. Specifically, a cost of fresh water of 1 $\$/m^3$ was estimated based on 0.24 $/kWh as the electricity cost of CSP. Manesh et al. (2013) studied the optimal integration of site utility and MED+RO desalination plant based on a simultaneous exergetic and economic optimisation. Also, Weiner at al. (2015) modelled and optimised a hybrid MED+RO system. This confirmed that the MED+RO hybrid system can be more energy efficient than a standalone MED process and with a recovery ratio superior to a standalone RO process. Recently, a comprehensive mathematical model is developed by Sadri et al. (2017) to describe the MED_TVC+RO integrated system. Moreover, the performance of integrated process is maximised by using a Genetic Algorithm (GA) technique.

The net outcome of the above literature review already showed that much attention been paid on the integration of power and desalination technologies and consequent energetic and/or economic assessment of the process. However, up to the authors' knowledge, the implementation of an integrated hybrid system of MED_TVC process coupled with RO process, has not yet been fully investigated. Also, it has been noticed that a parametric sensitivity analysis of several operating conditions using a hybrid system of MED_TVC+RO processes has not yet been explored. Therefore, the aim of this paper was to propose and evaluate different configurations in the context of simple and full hybridization of MED_TVC+RO processes. Also, the integrated process performance and sensitivity analysis to be explored via modeling and simulation. To systematically conduct this aim, detailed mathematical models of both MED_TVC and RO processes are initially developed. The mathematical models have been used to predict the performance of both MED_TVC and RO processes with a minimum amount of assumptions and limitations, which is rarely in other literature studies. This results in accurate models also the one developed for the hybrid process. Occasionally, most studies neglected the TVC section, which can be important to increase the performance ratio of the thermal process. The models developed of MED_TVC and RO process are individually validated against the predictions of several previous models of MED and the projected data collected from Toray Design System 2.0 (TDS2) for RO, respectively. Then, five different configurations have been designed to explore the best one in terms of productivity, fresh water quality, energy efficiency and recovery ratio of the whole hybrid process. A parametric sensitivity analysis with respect to seawater conditions and steam available from the power plant has been carried out in four of the proposed configurations. The output variables under investigation are the fresh water productivity, fresh water purity, energy consumption, and recovery ratio of the hybrid plant.

2. Description of the process

The description of both MED_TVC and RO processes is provided in Sections S.F.1 and S.F.2 in the supplementary file, respectively. In this respect, the schematic diagrams of forward feed multiple effect desalination process with thermal vapor compression and an industrial full-scale seawater RO desalination plant are given in Figs. S.F.1 and S.F.2 in the supplementary file, respectively.

Table 1 presents the technical specification and operating conditions of the MED and RO membrane processes. This also includes the permissible bounds of operating conditions of the membrane. The next section illustrates the description of the hybrid system of MED_TVC+RO.

Table 1. Specification and operating conditions of the MED and RO membrane processes

Operative parameter	Value	Unit
Number of effects	10	-
External steam flowrate	5.67	kg/s
Steam temperature	70	°C
Rejected brine temperature	40	°C
Rejected brine salinity	60	kg/m^3
Seawater temperature	25	°C
Seawater salinity	39	kg/m^3
External steam pressure	1300	kPa
Effective operating pressure in RO	50	atm
Membrane properties	**Value**	**Unit**
Membrane:	TM820M-400/ SWRO	-
Supplier	Toray membrane	-
Membrane material and module configuration	Polyamide thin-film composite Spiral wound element	-
Maximum operating pressure	81.91	atm
Maximum operating feed flow rate	0.00536	m^3/s
Minimum operating feed flow rate	0.001	m^3/s
Maximum pressure drop per element	0.987	atm
Maximum operating temperature	45	°C
Effective membrane area (A_m)	37.2	m^2
Module width (W)	37.2	m
Module length (L)	1	m
$A_{w\,(T_o)}$(m/ atm s) at 25 °C *	3.1591×10^{-7}	m/s atm
$B_{s(T_o)}$ NaCl (m/s) at 25 °C *	1.74934×10^{-8}	m/s
Spacer type	Naltex-129	-
Feed spacer thickness (t_f)	8.6×10^{-4} (34 mils)	m
Hydraulic diameter of the feed spacer channel d_h	8.126×10^{-4}	m
Length of spacer in the spacer mesh	2.77×10^{-3}	m
A' (dimensionless)	7.38	-
n (dimensionless)	0.34	-
ε (dimensionless)	0.9058	-

*: Estimated using parameter estimation in Section 3.2.2

2. Description of the Hybrid MED_TVC+RO process

Figs. 1 to 4 show the proposed configurations of the hybrid MED_TVC+RO process under investigation. In each configuration, the permeate of the RO membrane process is blended with the product of the thermal process, which is a distillate with a salinity close to zero. However, a value of 10 ppm is assumed for the salinity of the distillate to account a few seawater droplets that can be entrained in the vapor phase beyond the demisters. According to the World Health Organization

(WHO), the salinity of a good quality drinking water should be below 300 ppm, and precisely below 200 ppm for the most tap water (WHO, 2011). Therefore, the MED_TVC process has been designed to have a capacity approximately 4 times bigger than the RO process to produce enough distillate for the blending and commensurate with a salinity of the final product below 200 ppm. .

Fig. 1 shows the so-called simple hybridization of the thermal and pressure driven desalination processes. The seawater feed is split between the two processes, which operates unconnectedly. In other words, the operating conditions of one process have no effect on the other one, since the connection is only at the level of final products (fresh water) and rejected brine streams.

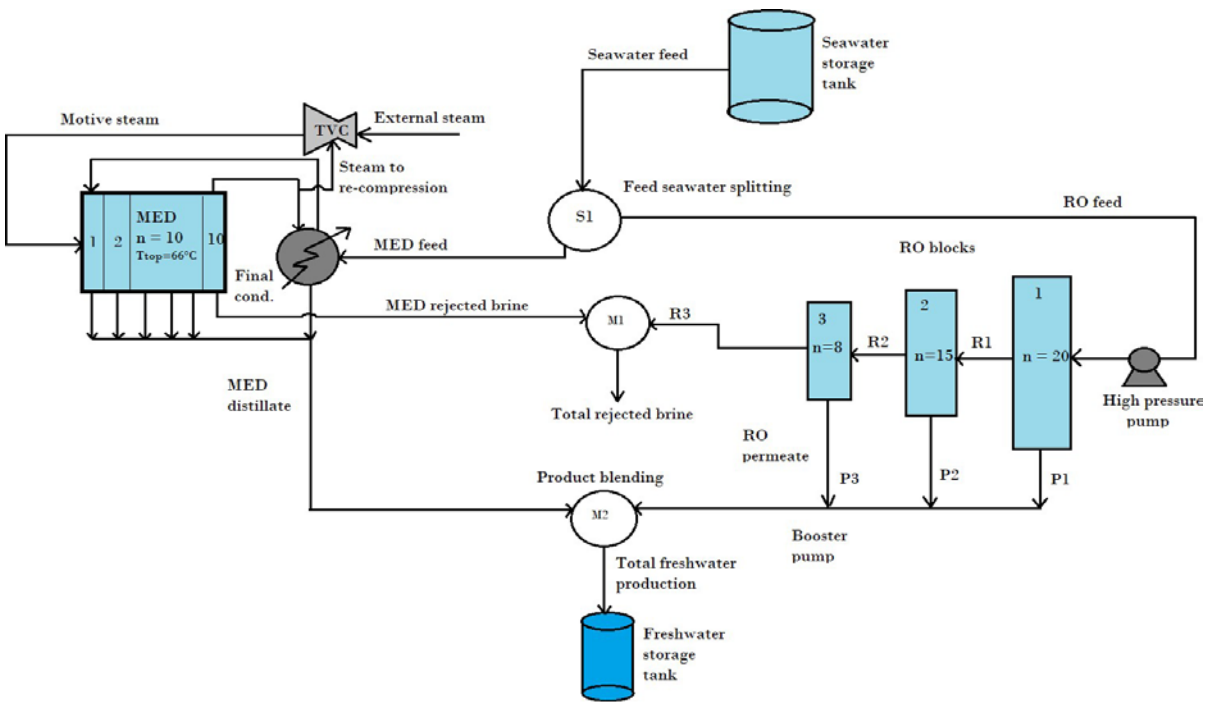

Fig. 1. Schematic diagram of the simple MED_TVC+RO hybridization.

Fig. 2 shows the full hybridization when the membrane process is placed upstream. This design has considered that the seawater feed is partially fed to the RO process and the rest is mixed with the retentate to form the inlet stream of the MED_TVC process. The option of blending a by-pass stream with the retentate is to accommodate the operating flow rate of MED_TVC process, which works at a greater capacity. Moreover, this option would reduce the feed salinity of the MED_TVC process. In this configuration, the rejected brine is made up only of the brine from the thermal process.

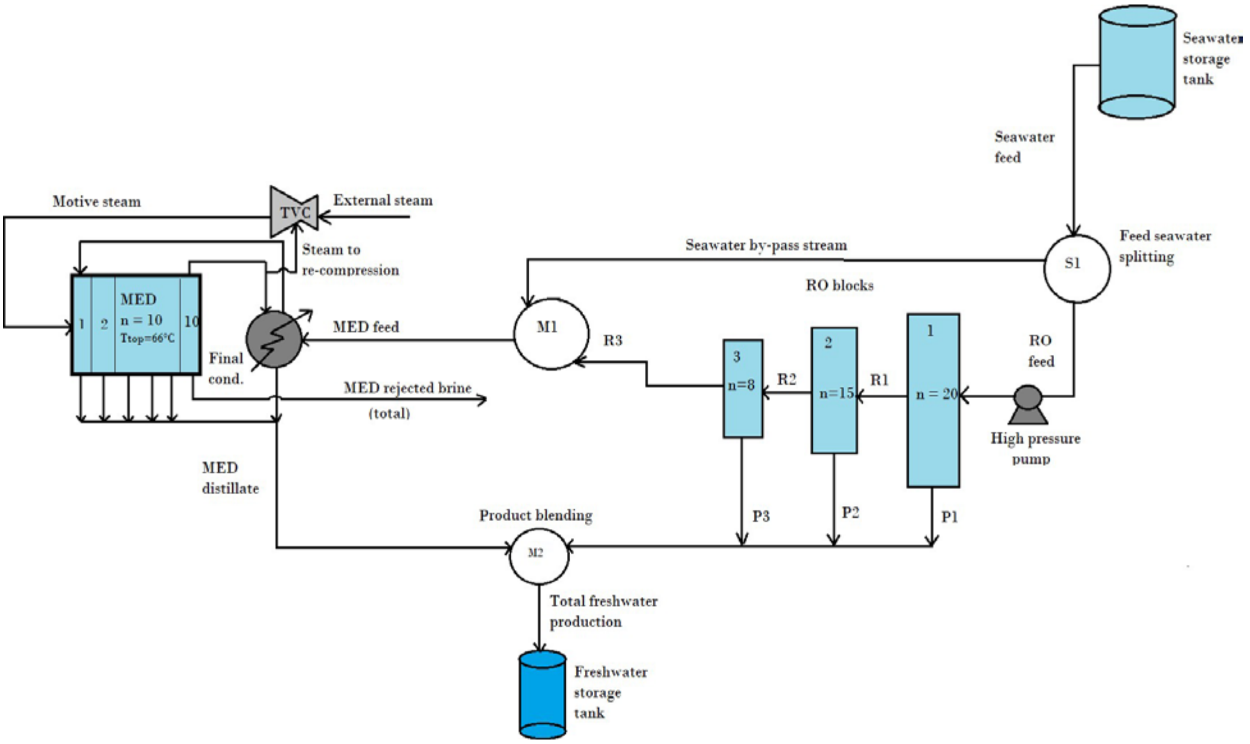

Fig. 2. Schematic diagram of full MED_TVC+RO system. RO process is upstream with respect to the MED process.

Another option for a full hybridization with the thermal MED_TVC process placed upstream is given in Fig. 3. In this configuration, the membrane process is fed with the rejected brine of the thermal process, which has a temperature of 40 °C and a salinity limited to 50 kg/m^3 to avoid a very fast membrane deterioration. As a result, the MED_TVC process is forced to operate in a small salinity window. The remaining brine of MED is blended with the RO retentate and rejected.

Finally, Fig. 4 shows the coupling of the MED process with a simple RO process of a single block comprises a total number of 43 of pressure vessels, where each pressure vessel includes 8 elements in series. Note that the total number of 43 pressure vessels has been already considered for other configurations, as well as the total seawater flow rate entering the membrane process.

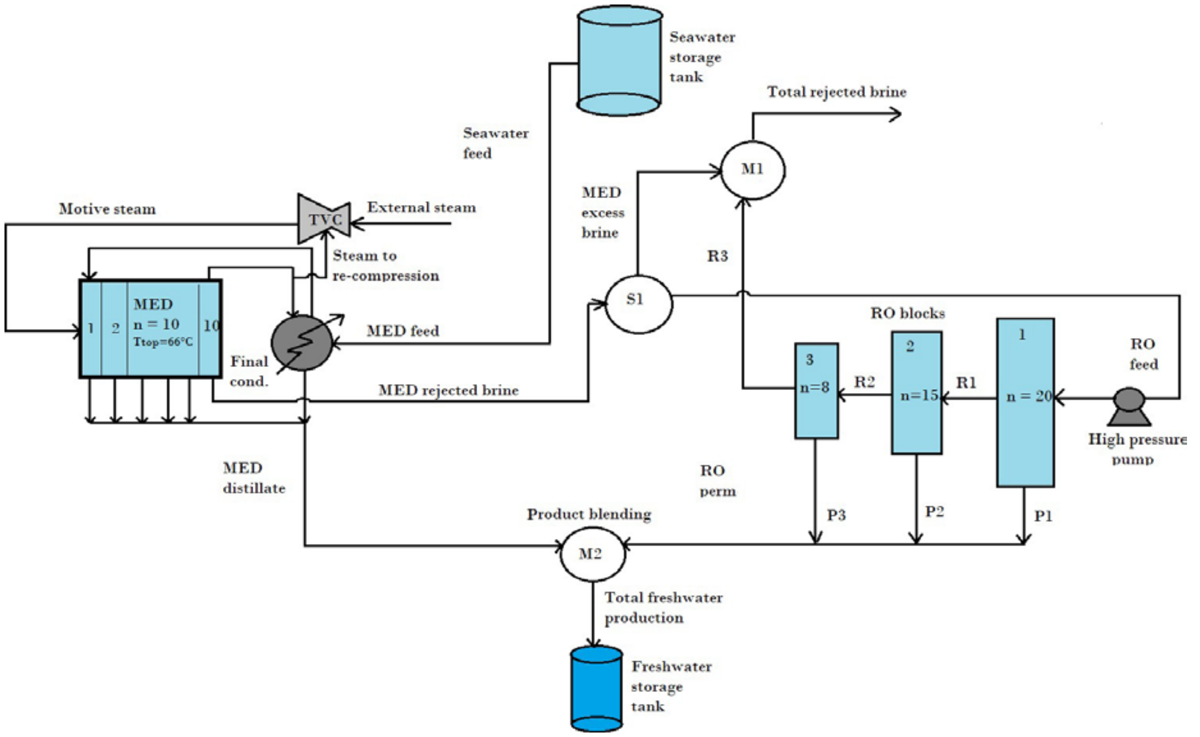

Fig. 3. Schematic diagram of full MED_TVC+RO system. MED process is upstream with respect to the RO process.

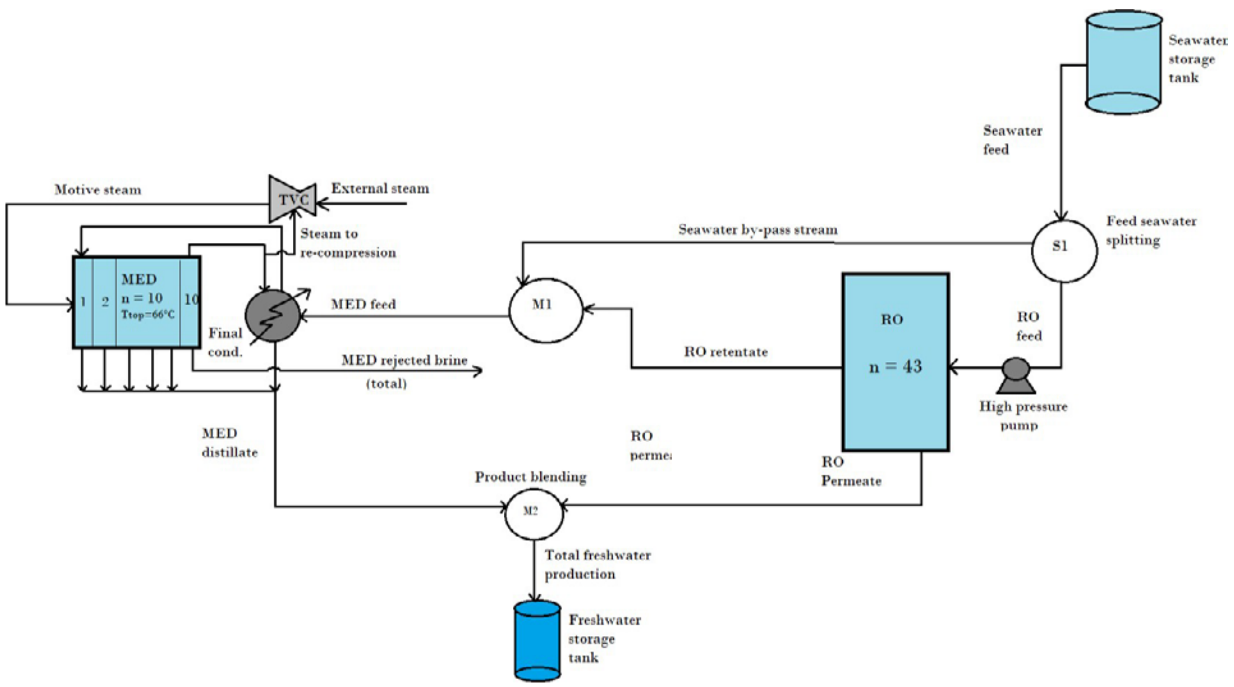

Fig. 4. Schematic diagram of full MED_TVC+RO system. RO process is upstream and made of a single block.

3. Model of the hybrid MED-RO process

The development of an accurate and detailed mathematical model is an importance target to express the essential phenomena of any industrial process, which enables to generate accurate results via simulation. In the next sections, the description of the models developed for the MED_TVC and RO processes is represented and followed by a validation study for each individual process.

3.1 MED_TVC process

The following model of MED process is adapted from Darwish et al. (2006). Interestingly, some modifications are made with respect to the original model. Specifically, detailed thermodynamic correlations are used to evaluate all the relevant thermodynamic properties of the system as a function of temperature, salinity, and fouling Note that all these characteristics were assumed as constants in the original work by Darwish et al. (2006). To accommodate the industrial reality, the equal exchange area of all the effects is imposed by means of a procedure for de-linearizing the temperature profiles. This new technique devised by the authors shows a very fast convergence, being able to approximately equalize area in a single iteration. The model for the thermal vapor compression section (TVC) is adapted from Dessouky et al. (2002) and given in Table A.1 in Appendix A.

3.1.1 Assumptions

1. Steady state process.
2. The vapour phase is salt free.
3. Energy loss to the surroundings is negligible.
4. Equal transfer area in all the effects.
5. Non-equilibrium allowance (NEA) and pressure drops are neglected.
6. Boiling point elevation and specific heat are considered as a function of temperature and salinity.

7. Latent heat of evaporation and overall exchange coefficient are considered as a function of temperature. For the heat exchange, experimental correlations that consider fouling are implemented.
8. Steam from the external utility is provided saturated and leaves as saturated liquid.

3.1.2 Model equations

The model is made of a series of material and energy balances together with the thermodynamics correlations, which are provided in the Appendix A. Steam flow rate *Ms* (kg/s) and steam temperature *Ts* (°C) are assumed to be known, since generated from an upstream process (i.e. a co-generation power plant or a renewable energy facility), while fresh water production is evaluated. The feed flow rate *Mf*, the total distillate flow rate *Md*, and the rejected brine flow rate *Mb* are evaluated according to simple overall material balances. Moreover, the salinity of the feed *xf* (kg/m^3) and of the rejected brine *xb* are known.

$$Md = Mf\ \frac{xb - xf}{xb}$$

(1)

$$Mb = Mf - Md$$

(2)

The sensible power $Q_{sensible}$ (kW) is used to heat the feed from the feed temperature after pre-heating *t1*, up to the boiling temperature in the first effect *T1*. The latent power Q_{latent} is used for vaporizing a quantity of distillate equal to *D1*, where $\lambda(Ts)$ is the latent heat of vaporization (kJ/kg) at steam temperature *Ts*.

$$Mf = \frac{Ms\ \lambda(Ts)}{Q_{sensible} + Q_{latent}}$$

(3)

$$Q_{sensible} = Mf \int_{t1}^{T1} cp(T1, x1)\, dT$$

(4)

$Q_{latent} = D1\,\lambda(Tv1)$

(5)

Linear temperature profiles can be defined as a *first attempt* by imposing an equal temperature drop (ΔT) among the effects and an equal temperature increase (Δt) among the feed pre-heaters, where Tb is the temperature of the rejected brine, equal to the temperature in the last effect. n is the number of effects.

$$\Delta T = \frac{T1-Tb}{n-1} \quad or\ \Delta T = \frac{Ts-Tb}{n} \qquad (6)$$

$\Delta T = \Delta t$

(7)

The feed temperature in the first effect (*t1*), after n-1 pre-heaters, can be evaluated starting from the temperature *tn* at the exit of the final condenser, which is assumed to be 11°C higher than seawater temperature. The temperature of the vapor phase *Tv* is lower than the brine temperature by the Boiling Point Elevation (*BPE*).

$t1 = tn + (n-1)\,\Delta t$

(8)

$Tv = T - BPE(T,x)$

(9)

A small fraction of brine rejected by each effect ($D_{flash,i}$) is flashed to a pre-heater for heating the feed stream. α is defined as the fraction of brine rejected by effect i-1 (B_{i-1}) that is flashed in the associated pre-heater, evaluated at mean temperature and salinity of the plant.

$D_{flash,i} = \alpha B_{i-1}$

(10)

$\alpha = \frac{cp(T_{mean},x_{mean})\Delta T}{\lambda(T_{mean})}$

(11)

Where $T_{mean} = \frac{T1+Tb}{2}$, $x_{mean} = \frac{xf+xb}{2}$ (12, 13)

The fraction of the total distillate produced by evaporation in each effect will be denoted as β. This value can be evaluated as a function of known parameters (number of stages, initial salinity, final salinity, α) by rearranging the material balances as follows;

$$D1 = D_{flash1} + D_{boil1} = \alpha Mf + \beta Md$$
$$B1 = Mf - D1 = (1-\alpha) Mf - \beta Md$$
$$D2 = D_{flash2} + D_{boil2} = \alpha B1 + \beta Md$$

$$B2 = B1 - D2 = (1-\alpha) B1 - \beta Md$$
$$B2 = (1-\alpha)[Mf(1-\alpha) - \beta Md] - \beta Md$$
$$B2 = (1-\alpha)^2 Mf - \frac{\beta Md}{\alpha}[1-(1-\alpha)^2]$$

Similarly, the brine rejected stream of the last effect can be evaluated with the following equation:

$$Bn = Mb = (1-\alpha)^n Mf - \frac{\beta Md}{\alpha}[1-(1-\alpha)^n]$$

(14)

Substituting Eq. (1) and (2) in Eq. (14), yields:

$$\frac{xb-xf}{xb} - 1 = \frac{xb-xf}{xb}(1-\alpha)^n - \frac{\beta}{\alpha}[1-(1-\alpha)^n]$$

(15)

Eq. (15) can be re-arranged to explicit the parameter β:

$$\beta = \frac{\alpha[xb(1-\alpha)^n - xf]}{(xb-xf)[1-(1-\alpha)^n]}$$

(16)

Accordingly, the amount of distillate boiled in each effect $D_{boiled,i}$, the total distillate (*Md*), and the brine flow rates B_i can now be evaluated, as well as the salinity profile.

$$D_{boiled,i} = \beta Md \quad (17)$$

$$D_i = D_{boiled,i} + D_{flash,i} \quad (18)$$

$B_i = B_{i-1} - D_i$

(19)

$x_i = \frac{x_{i-1} B_{i-1}}{B_i}$

(20)

The thermal loads in every effect Q_i (kW) and exchange areas of evaporators $A_{ev,i}$ (m^2) and pre-heaters $A_{ph,i}$ can be estimated using a simple energy balance, where U_{ev} is the overall heat exchange coefficient.

$Q_i = U_{ev,i} A_{ev,i} \Delta T_{ev,i}$

(21)

$Q_i = D_{boiled,i-1} \lambda(T_{v,i-1})$

(22)

$\Delta T_{ev,i} = Tv_{i-1} - T_i = T_{i-1} - BPE_{i-1} - T_i = \Delta T - BPE_{i-1}$

(23)

In the first effect, the thermal load Qs is directly provided by the external steam;

$Qs = Ms \cdot \lambda(Ts) = A_{ev,1} U_{ev,1} (Ts - T1)$

(24)

In the feed pre-heaters, heat exchange is between the flashed distillate at temperature Tv_i and liquid feed stream at a temperature t_i.

$Mf \cdot \int_{t_{i+1}}^{t_i} cp(t, xf)\, dt = U_{ph,i} A_{ph,i} \Delta t_{\log,i}$

(25) $\Delta t_{\log,i} = \frac{\Delta t}{\log\left(\frac{Tv_i - t_{i+1}}{Tv_i - t_i}\right)}$

(26) Since the exchange areas are evaluated using linear temperature profiles presented in Eq. (6), it is impossible to guarantee the fulfilment of Assumption 5, where equal area in all the

effects is assumed (Assumption 4). Therefore, temperature profiles can be de-linearized according to the following procedure devised by the authors to achieve a fast equalization of exchange areas. First, mean area of evaporators is evaluated using Eq. (27). Eq. (28) is solved by modifying the value of the vectors $\Delta T_{ex,i}$. Finally, Eq. (29) is solved to evaluate the vector ΔT_i which can be used to calculate the new non-linear temperature profiles.

$$A_{ev,mean} = \frac{\sum_{i=1}^{n} A_{ev,i}}{n} \tag{27}$$

$$A_{ev,mean} - \frac{Q_i}{U_{ev,i} \Delta T_{ex,i}} = 0 \tag{28}$$

$$\Delta T_i = \Delta T_{ex,i} - BPE_i \tag{29}$$

$$T_i = T_{i-1} - \Delta T_i \tag{30}$$

$$Tv_i = T_i - BPE\,(T_i, X_i) \tag{31}$$

All the process variables are then re-evaluated considering the new temperature profiles. The equality of areas is checked according to Eq. (32).

$$\Delta A_{ev}\% = \frac{\max(A_{ev}(2{:}10)) - \min(A_{ev}(2{:}10))}{A_{ev,mean}} \cdot 100\%$$

(32)

This procedure has been proved as an effective method to quickly equalizing the areas. In this respect, Table 2 shows the percentage error drops from 13.28 % to 0.76 % for the evaporator areas after a single iteration. However, the first effect is exempted, since it receives a different thermal load being the temperature difference between steam and brine in the first effect fixed at 4°C.

Table 2. Exchange areas in evaporators. Subscript *old* means before the equalizing procedure. Parameters for simulation are set according to Table 1.

Effect number	$A_{ev,old}$ [m^2]	A_{ev} [m^2]
Effect 1	1893.9834	1893.9834
Effect 2	2229.3867	2302.6501
Effect 3	2256.7415	2301.7188
Effect 4	2285.8877	2300.9355
Effect 5	2317.0193	2300.3308
Effect 6	2350.3570	2299.9404
Effect 7	2386.1506	2299.8086

Effect 8	2424.6880	2299.9875
Effect 9	2466.3015	2300.5405
Effect 10	2511.3794	2301.5420
Error %	**13.28 %**	**0.76%**

After the equalizing procedure, it is possible to proceed with the thermal vapor compression (TVC) section modeling. All the equations are summarized in Table A.1 in the Appendix A.

The last part of the process to be modelled is the final condenser, which receives a vapor flow rate (M_{COND}) to be condensed equal to the distillate from the last effect (D_n) minus the vapor fraction entrained in the TVC section (M_{TVC}).

$$M_{TVC} = Ms - Mm$$

(40)

$$M_{COND} = D_n - M_{TVC} \quad (41)$$

In the final condenser the seawater flow rate is heated up to a fixed temperature, exchanging the latent heat Q_{COND} provided by the condensation of steam. The unit can be modelled like a bigger pre-heater. Eq. (42) and (43) are used to evaluate the area of the final condenser A_{COND} and the total seawater flow rate Mw at temperature Tw, which is required by the MED. Indeed, the required flow rate is important to know, especially when it is provided by the RO process placed upstream, to design properly the by-pass stream.

$$Q_{COND} = U_{COND} A_{COND} \Delta T_{log,COND} \quad (42)$$

$$Q_{COND} = M_{COND} \lambda(Tv_n)$$

(43)

$$Q_{COND} = M_w \int_{Tw}^{tn} cp(T, xf)\, dT$$

(45)

$$\Delta T_{\log,COND} = \frac{tn - Tw}{\log\left(\frac{Tv_n - Tw}{Tv_n - tn}\right)}$$

(44)

3.1.3 Validation of MED process

The accuracy of any developed model should be tested before implementing the model in any parametric sensitivity analysis. Thus, the model developed in Section 3.1 of MED_TVC must be first computed and validated with the results of those from the literature. Specifically, the model validation has been carried out in terms of Gained Output Ratio (GOR) by comparing the prediction of the model developed against the prediction of other consolidated literature models, namely Dessouky et al. detailed (1998), El-Sayeh et al. (2001), Dessouky et al. simplified (2002), Darwish et al. (2006), and Mistry et al. (2012). The GOR is defined as the quantity of distilled fresh water (*Md*) produced by the process over the quantity of steam utilized (*Ms*) as an external utility in the first effect. More importantly, the model validation is carried out in the feasible range of 60 – 80 °C of steam temperature. The reason behind this is that running the MED process at low temperatures would require high exchange area, while a significant drop in the process performance is occurred at elevated steam temperatures (Dessouky et al., 2002). Table 3 shows that the prediction of the current model is closer to the one of an adaptive model of Mistry et al. (2012). Having said this, an acceptable convergence is noticed after comparing the recent model against El- Sayed et al. (2001) and Darwish et al. (2006) models. However, significant discrepancies are revealed after comparing the recent model against the models of Dessouky et al. detailed (1998), and Dessouky et al. simplified (2002). This can be ascribed to severe thermodynamics assumptions were made to develop the latterly models. Consequently, it is fair to say that the recent model developed is accurately able to predict the performance of MED due to low deviations of only 1.13-1.85% compared to the latest literature model. However, it is important to mention that this comparison has referred to the MED process without TVC. Therefore, the TVC section has been deactivated.

Table 3. Comparison of the present model with respect to literature model regarding GOR, for different steam temperatures, in the range of feasible values for low-temperature MED process.
Parameters for simulation: n=8, Tn=40°C, Tw =25°C, xf=42000 ppm, xn=70000 ppm.

Gained Output Ratio (GOR)											
	Present	Dessouky et		El-Sayed		Dessouky et		Darwish		Mistry	

ure (°C)

		model	al. (1998) detailed	% error	et al. (2001)	% error	al. (2002) simple	% error	et al. (2006)	% error	et al. (2012)	% error
	60	7.06	6.33	10.34	6.72	4.82	7.90	-11.90	7.44	-5.38	6.98	1.13
	62	7.001	6.21	11.33	6.68	4.53	7.88	-12.56	7.33	-4.73	6.917	1.20
	64	6.942	6.09	12.33	6.65	4.25	7.86	-13.22	7.22	-4.07	6.854	1.27
	66	6.883	5.96	13.35	6.61	3.95	7.84	-13.90	7.12	-3.39	6.791	1.34
	68	6.824	5.84	14.39	6.57	3.66	7.82	-14.60	7.01	-2.71	6.728	1.41
	70	6.765	5.72	15.45	6.54	3.36	7.80	-15.30	6.90	-2.01	6.665	1.48
	72	6.706	5.60	16.52	6.50	3.05	7.78	-16.02	6.79	-1.30	6.602	1.55
	74	6.647	5.48	17.62	6.47	2.74	7.76	-16.74	6.69	-0.58	6.539	1.62
	76	6.588	5.35	18.73	6.43	2.42	7.74	-17.49	6.58	0.16	6.476	1.70
	78	6.529	5.23	19.87	6.39	2.09	7.72	-18.24	6.47	0.91	6.413	1.78
	80	6.47	5.11	21.02	6.35	1.82	7.70	-19.01	6.36	1.64	6.35	1.85

3.2 RO process

The model developed in this paper for an individual spiral wound RO process is based on the model of Abbas (2005) that originally based on the principles of the solution diffusion model suggested by Lonsdale et al. (1965) to express the transport phenomena of water and solute through the membrane. The model developed is formerly considered the following assumptions:

1. The membrane characteristics and the channel geometries are assumed constant.
2. The film theory model is used to express the concentration polarisation.
3. Constant pressure of 1 atm at the permeate channel.
4. Isothermal process.

1. The correlation of Da Costa et al. (1994) is used to elucidate the pressure drop in the membrane feed channel.

Interestingly, several modifications are made on the model of Abbas (2005) as follows:

- Considering the impact of operating temperature on the membrane transport parameters using the proposed correlations of Toray membrane;
- The permeate concentration is estimated based on Al-Obaidi et al. (2017b), which is developed to consider solute transport parameter;
- The variation of physical properties against feed concentration and temperature is considered based on the developed correlations of Koroneos (2007) compared to constant physical properties assumed by Abbas (2005).

3.2.1 Model equations

The water Q_p (m³/s) and solute Q_s (kg/m² s) fluxes through the membrane are calculated as

$$Q_p = A_{w(T)} \left(P_f - \frac{\Delta P_{drop,E}}{2} - P_p - \pi_w - \pi_p\right) A_m$$

(46)

$$Q_s = B_{s(T)} (C_w - C_p)$$

(47)

$A_{w(T)}, P_f, \Delta P_{drop,E}, P_p, \pi_w, \pi_p, A_m, B_{s(T)}, C_w, C_p$ are water permeability constant at operating temperature (m/s atm), feed pressure (atm), pressure drop along the membrane element (atm), permeate pressure (atm), osmotic pressure at the membrane surface and permeate channel (atm), effective membrane area (m²), solute transport parameter at operating temperature (m/s), membrane wall concentration (kg/m³), and permeate concentrations (kg/m³), respectively. The osmotic pressure is calculated as (Abbas, 2005)

$$\pi_w = 0.76881\, C_w$$

(48)

$$\pi_p = 0.7994\, C_p$$

(49)

The impact of temperature T (°C) on transport parameters is calculated based on the transport parameters of water and solute at the reference temperature (Toray membrane)

$$A_{w(T)} = A_{w(25\ C)} \exp[0.0343\,(T - 25)] \qquad < 25\ °C$$

(50)

$$A_{w(T)} = A_{w(25\ C)} \exp[0.0307\,(T - 25)] \qquad > 25\ °C$$

(51)

$$B_{s(T)} = B_{s(25\ C)} \,(1 + 0.08\,(T - 25)) \qquad < 25\ °C$$

(52)

$$B_{s(T)} = B_{s(25\,C)}\ (1 + 0.05\,(T - 25)) \qquad > 25\ °C$$

(53)

The pressure drop $\Delta P_{drop,E}$ (atm) per element is calculated as proposed by Da Costa et al. (1994),

$$\Delta P_{drop,E} = \frac{9.8692x10^{-6}\, A' \rho_b\, {Q_b}^2\, L}{2 d_h\, Re^{n}\, (W\, t_f\, \epsilon)^2}$$

(54)

A', ρ_b, Q_b, L, d_h, Re_b, n, W, t_f and ϵ are the feed spacer characteristic (-), bulk density (kg/m³), bulk flow rate (m³/s), membrane length (m), the hydraulic diameter of the feed spacer channel (m), Reynolds number (-), feed spacer characteristic (-), membrane width (m), feed channel height (m), and the membrane porosity (-), respectively.

$$Re_b = \frac{\rho_b\, d_h\, Q_b}{t_f\, W\, \mu_b}$$

(55)

$$Q_b = \frac{Q_f + Q_r}{2} \qquad (56)$$

μ_b, Q_f, Q_r are kinematic viscosity (kg/m s), feed and retentate flow rates (m³/s), respectively. The bulk concentration C_b (kg/m³) is the average of feed C_f (kg/m³) and retentate C_r (kg/m³) concentrations as can be shown in Eq. (57)

$$C_b = \frac{C_f + C_r}{2}$$

(57)

The membrane surface concentration C_w (kg/m³) is expressed by the film theory model developed by Michaels, 1968 which is corresponding to the mass transfer coefficient k (m/s) (Da Costa et al., 1994)

$$\frac{(C_w - C_p)}{(C_b - C_p)} = exp\left(\frac{Q_p/A_m}{k}\right)$$

(58)

$$k = 0.664\, k_{dc}\, Re_b^{0.5}\, Sc^{0.33} \left(\frac{D_b}{d_h}\right) \left(\frac{2 d_h}{L_f}\right)^{0.5}$$

(59)

$$Sc = \frac{\mu_b}{\rho_b D_b}$$

(60)

k_{dc}, Sc, D_b, L_f are constant (-), Schmidt number (-), diffusivity parameter (m²/s), and length of filament in the spacer mesh (m), respectively. The physical properties of seawater are calculated based on Koroneos (2007).

$$\rho_b = 498.4\, m_f + \sqrt{[248400\, m_f^2 + 752.4\, m_f\, C_b]}$$

(61)

$$m_f = 1.0069 - 2.757x10^{-4}\, T \qquad (62)$$

$$D_b = 6.72510^{-6}\, exp\left\{0.154610^{-3}\, C_b - \frac{2513}{T+273.15}\right\} \qquad (63)$$

$$\mu_b = 1.234x10^{-6}\, exp\left\{0.0212\, C_b + \frac{1965}{T+273.15}\right\} \qquad (64)$$

The total mass and solute balance of the whole unit gives

$$Q_f = Q_r + Q_p \qquad (65)$$

$$Q_f\, C_f - Q_r\, C_r = Q_p\, C_p \qquad (66)$$

The permeate concentration C_p (kg/m³) is estimated by the correlation of Al-Obaidi et al. (2017b)

$$C_p = \frac{B_s\, C_f\, e^{\frac{J_w}{k}}}{J_w + B_s\, e^{\frac{J_w}{k}}} \qquad (67)$$

J_w denotes the water flux through the membrane (m/s). The overall solute rejection and recovery rate are

$$Rej = \frac{C_f - C_p}{C_f} \qquad (68)$$

$$Rec = \frac{Q_p}{Q_f} \qquad (69)$$

The above completed simulation model of an individual spiral wound RO process is used to build the full modelling package of the proposed configurations of multi-stage RO process including retentate reprocessing design of Fig. S.F.2 (given in the supplementary file). Table A.2 show the simulation model of the proposed configurations of multi-stage RO process, including the overall plant performance of solute rejection and total recovery and the interconnected streams of three blocks for retentate reprocessing design. Moreover, the model encompasses the calculation of product concentration, retentate concentration, and overall energy consumption. Finally, the model code is written and solved using gPROMS model builder software (general Process Modelling System by Process System Enterprise Ltd., 2001). The gPROMS environment can be used as a modelling platform for the steady state and dynamic simulation, optimisation, experiment design and parameter estimation.

3.2.2 Estimation of unknown model parameters

The RO model developed in Section 3.2.1 contains two unknown transport parameters of water and NaCl permeability constants at 25 °C ($A_{w(25\,C)}, B_{s(25\,C)}$) that will be used with the known parameters to solve the model equations. The gEST parameter estimation tool of gPROMS is used to investigate these parameters based on the projected data from the Toray Design System 2.0 (TDS2) that is a commercial projection software provided by the membrane manufacturer, i.e., Toray. Therefore, a set of projected data is gathered from TDS2 for a single pressure vessel holds eight membranes type TM820M-400/ SWRO (Toray) connected in series at several operating conditions. The estimated transport parameters are given in Table 1.

3.2.3 Validation of RO process

Table 4 shows the consistency between the model predictions of several operating parameters against the projected data of TDS2 at relatively small errors in the most parameters. Upon investigation of the validity of RO process model, it is fair to say that this model is valid enough to be augmented with the model of MED_TVC to represent the modelling of the hybrid process of MED_TVC+RO.

Table 4. RO model validation against TDS2 data

No.	Parameter	EXP	Model	Error%	No.	Parameter	EXP	Model	Error%	No.	Parameter	EXP	Model	Error%
1	Q_f/0.0197	C_f/35	T/25	P_f/55.91	5	Q_f/ 0.0099	C_f/35	T/25	P_f/50.35	9	Q_f/0.0066	C_f/35	T/25	P_f/51.1
	Q_r	0.0181	0.018	-0.80		Q_r	0.0083	0.0083	0.00		Q_r	0.005	0.005	-0.25
	C_r	38.03	37.779	0.66		C_r	41.65	41.412	41.65		C_r	46.02	46.041	-0.05
	C_p	0.1186	0.132	-11.38		C_p	0.1079	0.1314	0.10		C_p	0.1173	0.135	-15.13
	Q_p	0.0016	0.001	9.09		Q_p	0.0016	0.0015	0.00		Q_p	0.0016	0.001	0.78
	P_r	38.2	32.896	13.88		P_r	43.95	43.434	43.95		P_r	47.76	47.819	-0.12
	Rec	8	7.382	7.71		Rec	16	15.533	16		Rec	24	24.052	-0.21
	Rej	99.661	99.622	0.03		Rej	99.691	99.624	0.06		Rej	99.664	99.614	0.05
2	Q_f/0.0158	C_f/35	T/25	P_f/53.91	6	Q_f/0.0088	C_f/35	T/25	P_f/50.34	10	Q_f/0.0061	C_f/35	T/25	P_f/51.53
	Q_r	0.0142	0.014	-0.25		Q_r	0.0072	0.007	-0.62		Q_r	0.0045	0.004	-0.10
	C_r	38.875	38.829	0.12		C_r	42.66	42.482	0.41		C_r	47.26	47.347	-0.19
	C_p	0.1202	0.124	-3.87		C_p	0.11	0.131	-19.82		C_p	0.1202	0.136	-13.59
	Q_p	0.0016	0.001	2.30		Q_p	0.0016	0.001	2.828		Q_p	0.0016	0.001	0.28
	P_r	40.79	38.231	6.27		P_r	45.02	44.750	0.59		P_r	48.61	48.706	-0.19
	Rec	10	9.893	1.06		Rec	18	17.667	1.84		Rec	26	26.153	-0.59
	Rej	99.656	99.643	0.01		Rej	99.685	99.623	0.06		Rej	99.656	99.609	0.04
3	Q_f/0.0131	C_f/35	T/25	P_f/52.87	7	Q_f/ 0.0079	C_f/35	T/25	P_f/50.48	11	Q_f/0.0056	C_f/35	T/25	P_f/52.05
	Q_r	0.0116	0.011	1.07		Q_r	0.0063	0.0063	-0.51		Q_r	0.0041	0.004	2.41
	C_r	39.76	39.937	-0.45		C_r	43.72	43.63	0.21		C_r	48.56	48.933	-0.76
	C_p	0.122	0.122	-0.04		C_p	0.1123	0.1326	-18.15		C_p	0.1234	0.138	-12.51
	Q_p	0.0016	0.001	-1.53		Q_p	0.0016	0.0015	2.03		Q_p	0.0016	0.001	0.05
	P_r	42.62	41.592	2.40		P_r	45.98	45.891	0.19		P_r	49.47	49.655	-0.37
	Rec	12	12.401	-3.34		Rec	20	19.840	0.79		Rec	28	28.554	-1.98
	Rej	99.651	99.651	0.00		Rej	99.679	99.620	0.05		Rej	99.647	99.603	0.04
4	Q_f/0.0113	C_f/35	T/25	P_f/52.32	8	Q_f/0.0072	C_f/35	T/25	P_f/50.74	12	Q_f/0.0053	C_f/35	T/25	P_f/52.64
	Q_r	0.0097	0.009	0.53		Q_r	0.0056	0.005	-0.39		Q_r	0.0037	0.003	0.32
	C_r	40.68	40.972	-0.72		C_r	44.84	44.786	0.11		C_r	49.95	50.236	-0.58
	C_p	0.124	0.121	1.80		C_p	0.1147	0.133	-16.60		C_p	0.1268	0.139	-10.30
	Q_p	0.0016	0.001	-3.25		Q_p	0.0016	0.001	1.37		Q_p	0.0016	0.001	-0.74
	P_r	44.03	43.645	0.87		P_r	46.89	46.876	0.02		P_r	50.35	50.494	-0.28
	Rec	14	14.620	-4.43		Rec	22	21.917	0.37		Rec	30	30.414	-1.38
	Rej	99.645	99.652	-0.00		Rej	99.672	99.617	0.05		Rej	99.637	99.600	0.03

4. Modelling of the hybrid MED_TVC+RO processes

The earliest sections provided the validation of the models developed for the thermal and membrane processes. Therefore, it is possible to connect them in several ways to accommodate the proposed configurations, as illustrated in Section 2.

4.1 Simple hybridization

Referring to Fig. 1, simple material balances on mixers M1 and M2 are used to describe the blending of the rejected brine and fresh water. Md_{MED} is the distillate produced by the thermal process with a salinity xd_{MEd}, Mp_{RO} is the permeate produced by RO with a salinity xp_{RO}, and $M_{freshwater}$ is the total productivity of the plant, with a salinity equal to $x_{freshwater}$. Note that the salinity of the distillate from MED is always assumed equal to 10 ppm.

$$Md_{MED} + Mp_{RO} = M_{freshwater}$$

(70)

$$Md_{MED}xd_{MEd} + Mp_{RO}xp_{RO} = M_{freshwater}x_{freshwater}$$

(71)

It is also important to evaluate the flow rate of rejected brine M_{reject} as the sum of the rejected brine of the two processes, as well as its salinity x_{reject}. Note that the salinity of the rejected brine from MED is fixed at 60 kg/m^3.

$$Mb_{MED} + Mr_{RO} = M_{reject}$$

(71)

$$Mr_{MED}xr_{MED} + Mp_{RO}xr_{RO} = M_{reject}x_{reject}$$

(72)

4.2 Full Hybridization, RO upstream

Referring to Fig. 2, Eqs. (70) and (71) are used to evaluate the flow rate of fresh water produced by the plant and its purity, while the rejected brine is entirely produced by the MED process. For this configuration, it is necessary to quantify the by-pass flow rate M_{bypass} to provide the proper feed Mw_{MED} in the thermal process, with a salinity equal to xf_{MED}.

$$Mw_{MED} = Mr_{RO} + M_{bypass}$$

(73)

$$Mw_{MED}xf_{MED} = Mr_{RO}xr_{RO} + M_{bypass}x_{seawater}$$

(74)

4.3 Full Hybridization, MED upstream

Referring to Fig. 3, Eqs. (70) and (71) are used to evaluate the flow rate of fresh water produced by the plant and its purity. The rejected brine is evaluated accordingly to Eqs. (75) and (76), which model the blending of RO retentate and excess MED brine, where Mr_{RO} is the retentate from the membrane process and xr_{RO} its salinity. Note that the MED is now forced to produce a brine with a salinity of 50 kg/m^3, to obtain a suitable inlet condition for the RO process.

$$Mb_{MED} + Mr_{RO} - Mf_{RO} = M_{reject}$$

(75)

$$(Mr_{MED} - Mf_{RO})xr_{MED} + Mp_{RO}xr_{RO} = M_{reject}x_{reject}$$

(76)

4.4 Parameters for comparison

The comparison between the different proposed configurations is essentially based on the following chosen quantities: the productivity of the hybrid plant ($M_{freshwater}$), purity of the product ($x_{freshwater}$), specific energy consumption (*Es*), and recovery ratio (*RR*). A sensitivity analysis of those parameters has been performed. Also, the quantity of rejected brine (M_{reject}) and its salinity (x_{reject}) have been evaluated for every configuration, where this parameter is important for environmental reasons. The total energy is evaluated using Eq. (77) by considering the energy requirement of both processes. In this respect, the energy consumed by the thermal process is calculated by Eq. (78) and linked with the steam enthalpy that converted into kWh/m^3, where only a small fraction (E_{el} = 2 kWh/m^3) is considered as an electrical energy consumed by pumps (Gude et al., 2010). However, the electrical energy required by the membrane process is given by Eq. (79), which represents the required pumping energy to compress the feed up to 50 atm. Eq. (80) is used to estimate the total recovery ratio.

$$E_s = \frac{E_{s,MED} Md_{MED} + E_{s,RO} Mp_{RO}}{M_{freshwater}} \quad (77)$$

$$E_{s,MED} = \frac{M_{steam}\,\lambda(Ts)}{Md_{MED}} + E_{el} \quad (78)$$

$$E_{s,RO} = \frac{P_{RO} Mf_{RO}}{\eta_{pump} Mp_{RO}} \quad (79)$$

$$RR = \frac{M_{freshwater}}{M_{seawater}} \quad (80)$$

5. Results and discussion

In this section, a sensitivity analysis is performed to simultaneously compare the four proposed configurations and to investigate the variation of the parameters when external inputs such as seawater conditions and steam supply change for each considered configuration. A variation of ± 12% for steam consumption and seawater salinity and ± 8% of seawater temperature has been considered with respect to the initial values reported in Table 1, where also the operating conditions of MED and RO processes are reported. It is noteworthy to mention that a by-pass stream is necessary to satisfy the feed requirement of the thermal process, being the latter more productive, when the RO process is placed upstream. The by-pass ratio, defined as the quantity of seawater fed to the MED process over the quantity of seawater fed to the RO process, which is already calculated as a function of the operating conditions. Specifically, its value is around 3; this means that the by-pass stream is larger than the feed stream to the RO process by around three folds. Then, the simulation results are compared against the performance of other proposed configurations in terms of productivity, energy consumption, the purity of the product, and recovery ratio to identify the best one.

5.1 Sensitivity analysis

Performing a sensitivity analysis is important for the design and operation perspectives of any industrial process. This in turn would offer the feasible operating parameters that serve the process performance. Results obtained from the simulation of different configurations of MED_TVC+RO hybrid processes are shown in Figs. 5 – 10. These figures show the value of the performance indicators of the hybrid plant, in relation to the variation of the most important operating parameters. The selected performance indicators are at the same level of importance and commonly used in the literature.

Figs. 5 and 6 show the effect of steam supply variation of the MED process on the key performance indicators of hybrid system, i.e., the overall productivity and fresh water salinity.

This in turn confirmed that the production of fresh water linearly increases as well as its purity as a result to increasing the steam fed to the thermal process. Apparently, the hybrid plant productivity is, for every configuration, strongly dependent on the quantity of steam used. This is because the MED process accounts for approximately ¾ of the total fresh water production (Fig. 5).

The comparison of four proposed configurations based on the product salinity is investigated based on the steam consumption in Fig. 6. This in turn shows that the configuration with MED upstream generates a product with a salinity always above 300 ppm. Specifically, this is quite comparable to all the other proposed configurations, which produce fresh water with salinity under 200 ppm foe every operating condition. To systematically resolve this problem, a more productive MED plant should be designed to dilute even more the high-salinity RO permeate, or a different RO process structure must be implemented to generate a purer permeate.

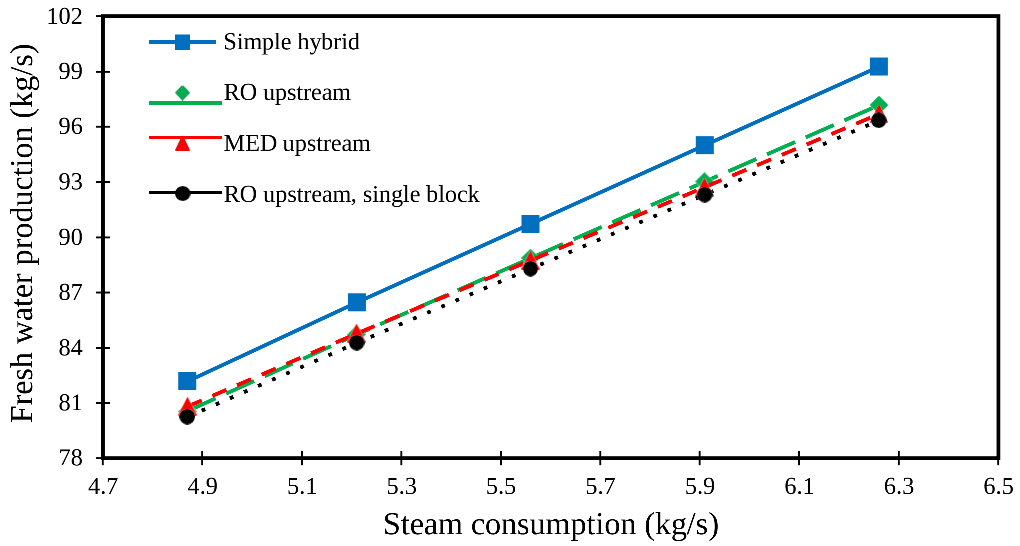

Fig. 5. Fresh water production versus steam consumption in the thermal process for different configurations of the hybrid process.

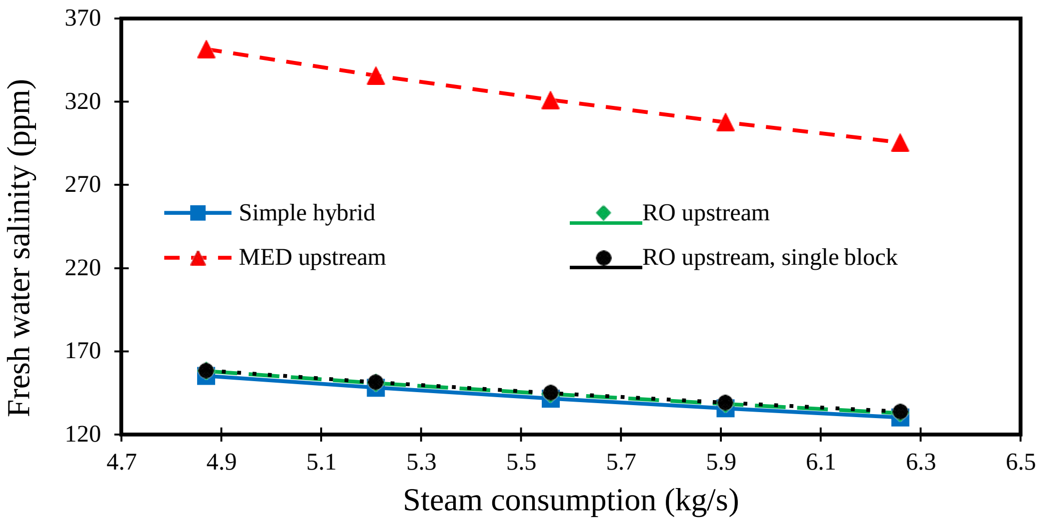

Fig. 6. Fresh water salinity versus steamconsumption in the thermal process for different plant configurations of the hybrid process.

The effect of seawater temperature variation on the fresh water productivity and energy consumption of the hybrid system is plotted in Figs. 7 and 8, respectively. The simple hybrid configuration presented in Fig. 1 is the least sensitive to variation of external seawater temperature, due to its simplicity and straightforward operation, while the configuration with MED upstream is the more sensible configuration. Specifically, Figs. 7 and 8 confirm that the simple hybrid configuration performs a slightly higher productivity and a little lower energy consumption. However, those advantages tend to invalidate at high seawater temperatures, which is the most realistic scenario when considering hot and arid regions as possible sites to install the proposed plant.

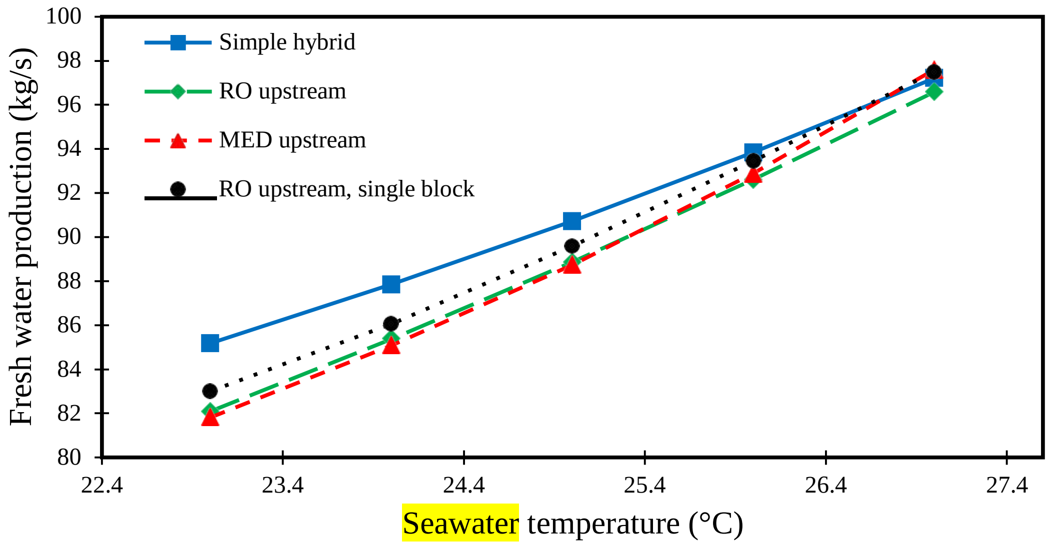

Fig. 7. Fresh water production versus inlet seawater temperature for different plant configurations of the hybrid process.

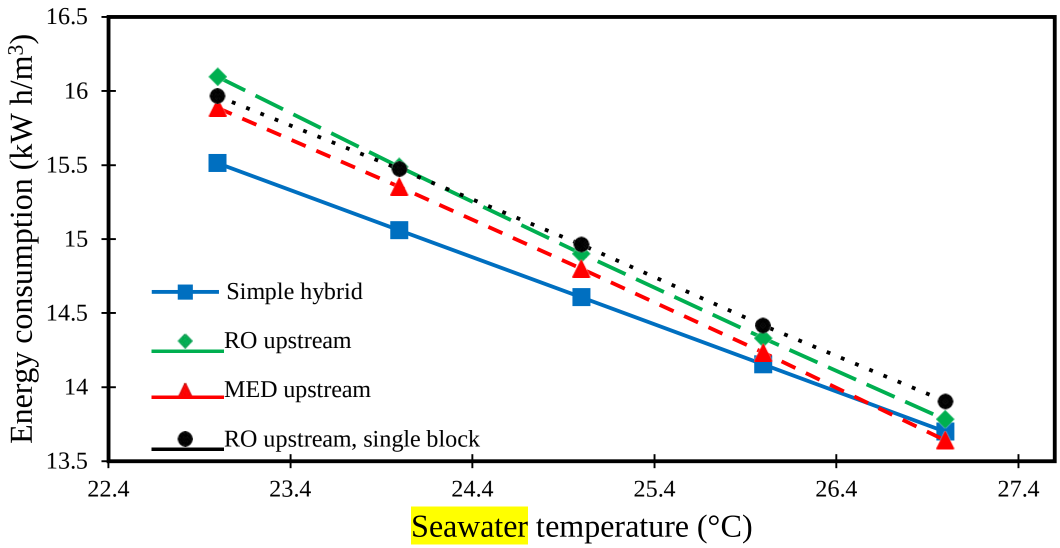

Fig. 8. Specific energy consumption versus inlet seawater temperature for different plant configurations ofthe hybrid process.

Figs. 9 and 10 show the effect of seawater salinity variation on the energy consumption and the overall recovery ratio of the hybrid system. The full hybrid configuration with RO upstream shows a relatively higher performance under every aspect for both the three blocks and single block configurations represented in Figs. 2 and 4, respectively. Specifically, Fig. 9 confirms the superiority of this configuration regarding the recovery ratio, except for very high seawater salinity (over 41 kg/m^3). The reason for this behavior is that all the rejected brine of the membrane process is re-utilized as feed for the thermal process, which reduces the need for an external seawater feed. In contrast, the full hybrid configuration with MED upstream has some issues related to the fact that the thermal process is forced to produce a lower salinity brine to feed the membrane process. Accordingly, this limits the salinity windows in which it can operate and thus reducing the MED upstream performance. This is especially true when seawater salinity is high (for instance, 40 – 43 kg/m^3). Moreover, the MED process operates very poorly at a noticeable increase of energy consumption (Fig. 9) and a significant reduction of the recovery ratio (Fig. 10). However, the MED upstream design allows to reach a considerable recovery ratio that commensurate with the lowest energy consumption if the seawater salinity is low (for instance 35 kg/m^3). Energy consumption is generally moderately dependent on seawater conditions, except for the MED upstream configuration, which shows a strong dependence (Figs. 8 and 10). Recovery ratio is linear dependent on seawater salinity for the simple hybridization (weakly) and MED upstream hybridization (strongly), while there is a moderate non-linear dependence for the RO upstream configurations (Fig. 9).

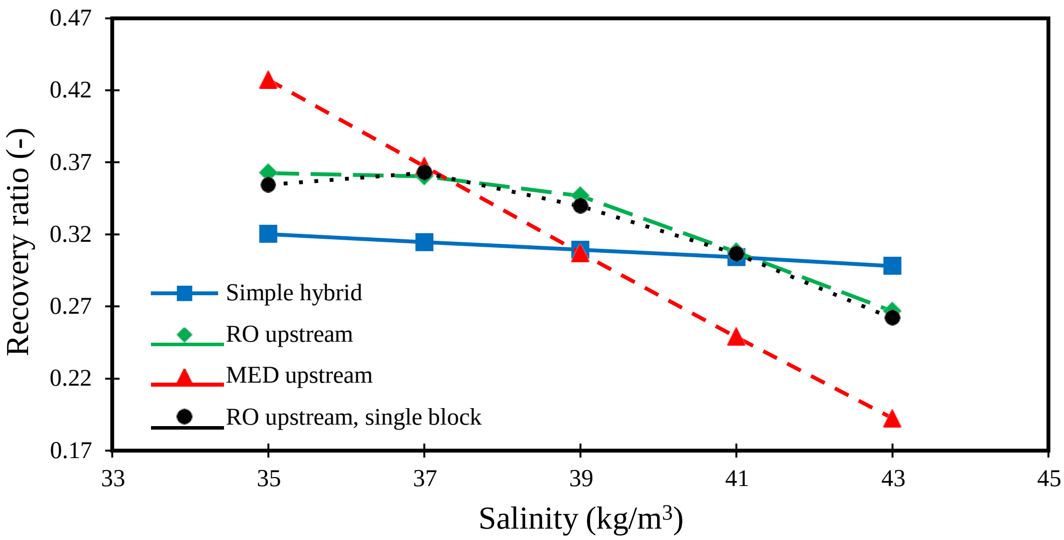

Fig. 9. Recovery ratio versus inlet seawater temperature for different plant configurations of the hybrid process.

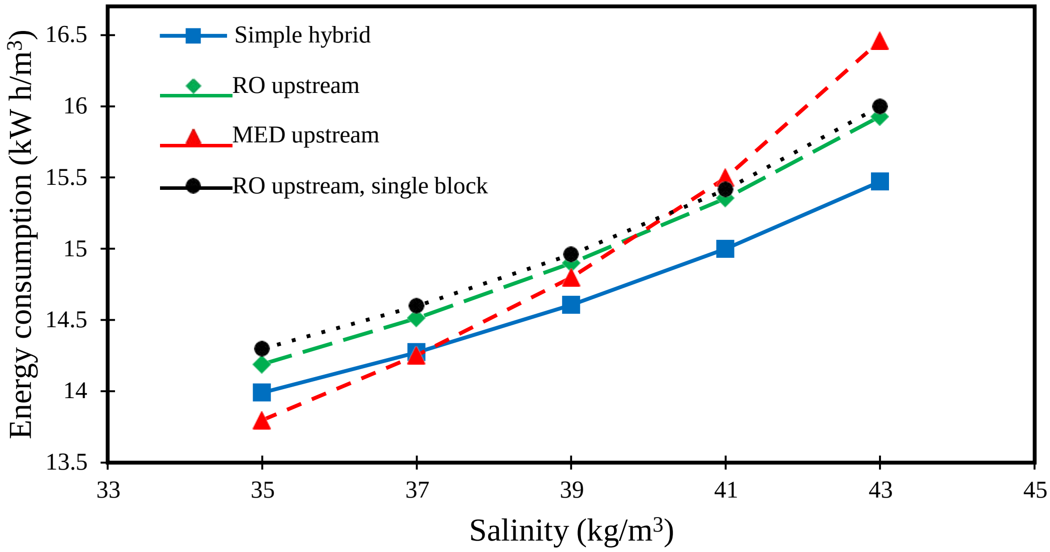

Fig. 10. Specific energy consumption versus inlet seawater temperature for different plant configurations of the hybrid process.

Table 5 presents the simulation results of all the proposed configurations with a fixed seawater salinity of 37 kg/m^3. All other parameters are set according to Table 1. Moreover, the evaluation of the flowrate and salinity of the rejected brine is included.

Table 5. Performance comparison of the proposed configurations. Simulations performed with seawater salinity of 37 kg/m^3, other parameters set accordingly with Table 1

Configuration type	Productivity (kg/s)	Product salinity (ppm)	Rejected flow (kg/s)	Rejected salinity (kg/m^3)	Energy Consumption (kW h/m^3)	Recovery Ratio (-)
Simple hybrid	93.36	136	162.84	60.72	14.27	0.3146
RO upstream	91.80	138	165.73	60.00	14.51	0.3603
RO upstream, 1 block	93.25	135	154.75	60.00	14.93	0.3521
MED upstream	92.42	306	198.17	53.08	14.25	0.3673

Table 5 shows how the configuration with MED upstream produces the highest brine flow rate despite attaining the lowest rejected salinity compared to other configurations. This is due to considering of 50 kg/m^3 as the rejected brine concentration of the thermal process instead of 60 kg/m^3 when placed upstream. Another relevant observation is that using the RO process in a single block can lead to a reduction of about 7% of the rejected flow rate compared to RO upstream configuration. Up to the authors' knowledge, this reduction is not enough to justify the feasibility of this configuration compared to the conventional 3 RO blocks, which presents higher recovery ratio and slightly lower energy consumption.

To investigate the robustness of the proposed hybrid system, the earlier simulation results are compared with the findings of a detailed study of MSF+RO hybrid plant carried out by Helal et al. (2004). Specifically, Helal et al. (2004) have investigated all the possible alternatives for integrating the thermal MSF process and the membrane RO process in a hybrid system. The authors also conducted an economic analysis to estimate the cost of fresh water for every proposed configuration. The output of this study has affirmed that the best configuration was the one where the RO and the MSF plants were partially integrated. In other words, a fraction of the heated feed from the intake was fed to the single-stage RO plant, then the RO permeate was mixed with the MSF distillate and the reject stream was combined with the MSF blowdown. This configuration was able to generate fresh water at around 500 ppm, with an overall recovery ratio of 32.4 %. Interestingly, the investigated MED_TVC+RO system in the current study is in turn able to generate fresh water with a salinity lower than 200 ppm, with an overall recovery ratio up to 37 %. However, the performance of this system is quite sensible to the variation of seawater properties. Most importantly, the current study explored the impact of possible variations of seawater properties (i.e. seasonal changes) on the hybrid process performance. According to our results, the best overall configuration appears to be the MED_TVC+RO full hybrid with RO process placed upstream This is due to the best recovery ratio over a wide range of seawater salinity, moderately dependence of other parameters on changing seawater conditions, and low salinity of the produced freshwater. No great differences are highlighted between the triple block RO upstream configuration and the single block configuration. However, the use of three separate blocks allows a slightly lower energy consumption. Finally, it can be said that the simple hybrid could be a more feasible option in case of operating at cooler and very low salinity seawater. However, this will not be the case because this kind of plants is usually installed in hot regions with fairly high seawater salinity (i.e. Gulf regions).

6. Conclusions

In this paper, the interest is on the MED_TVC+RO hybrid desalination systems, that are less well studied in the literature compared to other more popular hybrid configurations, such as MSF+RO. Detailed mathematical models for both the thermal and the membrane processes have been developed and validated against literature and projected data of TDS2, respectively, providing a good agreement. Four different possibilities to connect the processes have been investigated. Moreover, a performance sensitivity analysis of the proposed configurations was performed by running the simulations with variable seawater properties and steam supply. The productivity of the various configurations, the purity of the fresh water, recovery ratio, and energy consumption, were considered as the performance indicators. The results confirmed that placing the MED process upstream results unfeasible for a high seawater salinity due to bad operation of the thermal process, bounded in a narrow salinity window. In other words, the MED process upstream hybrid system is significantly sensible with respect to seawater salinity. Additionally, the generated fresh water salinity appears to be too high. On the other hand, placing the RO process upstream in a full hybridized configuration provides an enhanced recovery ratio for seawater salinity under 41 kg/m^3. This configuration proved to be competitive also from the point of view of productivity and energy consumption. Therefore, this configuration was identified as the best one overall among the four proposed configurations.

Appendix A

Collected from : El-Dessouky HT, Ettouney H.M., 2002. *Fundamentals of salt water desalination*. Elsevier.

Boiling Point Elevation

Correlation valid in the range: 1% < w < 16%, 10°C < T < 180°C

$$
\begin{aligned}
w &= x \cdot 10^{-5} \qquad [w / w\%] \\
BPEa &= 8.325 \cdot 10^{-2} + 1.883 \cdot 10^{-4} \cdot T + 4.02 \cdot 10^{-6} \cdot T^{2} \\
BPEb &= -7.625 \cdot 10^{-4} + 9.02 \cdot 10^{-5} \cdot T - 5.2 \cdot 10^{-7} \cdot T^{2} \\
BPEc &= 1.522 \cdot 10^{-4} - 3 \cdot 10^{-6} \cdot T - 3 \cdot 10^{-8} \cdot T^{2} \\
BPE &= BPEa \cdot w + BPEb \cdot w^{2} + BPEc \cdot w^{3} \qquad [°C]
\end{aligned}
$$

Specific heat at constant pressure

Correlation valid in the range: 20000 ppm < x < 160000 ppm, 20°C < T < 180°C

$$
\begin{aligned}
s &= x \cdot 10^{-3} \qquad [gm / kg] \\
cpa &= 4206.8 - 6.6197 \cdot s + 1.2288 \cdot 10^{-2} \cdot s^{2} \\
cpb &= -1.1262 + 5.4178 \cdot 10^{-2} \cdot s - 2.2719 \cdot 10^{-4} \cdot s^{2} \\
cpc &= 1.2026 \cdot 10^{-2} - 5.3566 \cdot 10^{-4} \cdot s + 1.8906 \cdot 10^{-6} \cdot s^{2} \\
cpd &= 6.8777 \cdot 10^{-7} + 1.517 \cdot 10^{-6} \cdot s - 4.4268 \cdot 10^{-9} \cdot s^{2} \\
cp &= \frac{cpa + cpb \cdot T + cpc \cdot T^{2} + cpd \cdot T^{3}}{1000} \qquad \left[\frac{kJ}{kg \cdot °C}\right]
\end{aligned}
$$

Latent heat of evaporation

$$\lambda = 2501.89715 - 2.40706 \cdot T + 1.19221 \cdot 10^{-3} \cdot T^{2} - 1.5863 \cdot 10^{-5} \cdot T^{3} \qquad \left[\frac{kJ}{kg}\right]$$

Global heat exchange coefficients

$$U_{ev} = 1.9695 + 1.2057 \cdot 10^{-2} \cdot T - 8.5989 \cdot 10^{-5} \cdot T^{2} + 2.5651 \cdot 10^{-7} \cdot T^{3} \qquad \left[\frac{kW}{m^{2} \cdot °C}\right]$$

$$U_{cond} = U_{ph} = 1.7194 + 3.2063\cdot10^{-3}\cdot T + 1.597\cdot10^{-5}\cdot T^{2} - 1.9918\cdot10^{-7}\cdot T^{3} \quad \left[\frac{kW}{m^{2}\cdot°C}\right]$$

Table A.1. Equations describing the TVC section modelling. Reference: Dessouky et al. (2002)

No.	Title	The Mathematical Expression
1	Pressure Correction Factor	$PCF = 3e-7\cdot Pm^{2} - 0.0009\cdot Pm + 1.6101$
2	Temperature Correction Factor	$TCF = 2e-8\cdot Tv_{n}^{2} - 0.0006\cdot Tv_{n} + 1.0047$
3	Pressure at vapor temperature	$Pv = P_{crit}\, e^{(\frac{T_{crit}}{Tv_n}+273.15)-1}\cdot\sum_{j=1}^{8} f_j$
4	Pressure at steam temperature	$Ps = P_{crit}\, e^{(\frac{T_{crit}}{Ts}+273.15)-1}\cdot\sum_{j=1}^{8} f_j$
5	Calculate Compression Ratio	$CR = \frac{Pv}{Ps}$
6	Calculate Entrainment Ratio	$Ra = 0.296\,\frac{Ps^{1.19}}{Pev^{1.04}}\,\frac{Pm^{0.015}}{Pev^{0.015}}\,\frac{PCF}{TCF}$
7	Calculate motive steam flowrate	$Mm = Ms\,\frac{Ra}{1+Ra}$

Effect number	$f1$	$f2$	$f3$	$f4$	$f5$	$f6$	$f7$	$f8$
Value	-7.4192	0.29721	-0.1155	0.00868	0.00109	-0.0043	0.00252	-0.00052

Table A.2. The mathematical modelling of retentate reprocessing RO desalination plant (Fig. S.F.2 in the supplementary file)

Model Equations	Specifications	Eq. no
$Q_{f(plant)} = Q_{r(plant)} + Q_{p(plant)}$	Plant feed flow rate	1
$Q_{f(plant)}\,C_{f(plant)} = Q_{r(plant)}\,C_{r(plant)} + Q_{p(plant)}\,C_{p(plant)}$	Plant feed concentration	2
$Q_{r(plant)} = Q_{r(Block\ 3)}$	Plant retentate flow rate	3
$C_{r(plant)} = C_{r(Block\ 3)}$	Plant retentate concentration	4
$C_{p(Plant)} = \frac{C_{p(Block\ 1)}Q_{p(Block\ 1)} + C_{p(Block\ 2)}Q_{p(Block\ 2)} + C_{p(Block\ 3)}Q_{p(Block\ 3)}}{Q_{p(plant)}}$	Plant product concentration	5
$Q_{p(Plant)} = Q_{p(Block\ 1)} + Q_{p(Block\ 2)} + Q_{p(Block\ 3)}$	Plant permeate flow rate	6
$T_{f(plant)} = T_{r(plant)}$	Plant constant temperature	7
$P_{f(plant)} = P_{f(Block\ 1)}$	Plant feed pressure	8
$P_{r(plant)} = P_{r(Block\ 3)}$	Plant retentate pressure	9
$Rec_{(plant)} = \frac{Q_{p(plant)}}{Q_{f(plant)}}\,x100$	Total plant permeate recovery	10
$Rej_{(plant)} = \frac{C_{f(plant)} - C_{p(plant)}}{C_{f(plant)}}\,x100$	Total plant rejection	11

$C_{f(Block\ 1)} = C_{f(plant)}$	Feed concentration of 1st block	12
$Q_{f(Block\ 1)} = Q_{f(plant)}$	Feed flow rate of 1st block	13
$Q_{p(Block\ 1)} = \sum_{PV=1}^{20} Q_{p(PV)}$	Permeate flow rate of 1st block	14
$C_{p(Block\ 1)} = \frac{\sum_{PV=1}^{20} C_{p(PV)}\ Q_{p(PV)}}{Q_{p(Block\ 1)}}$	Permeate concentration of 1st block	15
$Rej_{(Block\ 1)} = \frac{C_{f(Block\ 1)} - C_{p(Block\ 1)}}{C_{f(Block\ 1)}}\ x100$	Total solute rejection of 1st block	16
$Rec_{(Block\ 1)} = \frac{Q_{p(Block\ 1)}}{Q_{f(Block\ 1)}}\ x100$	Total permeate recovery of 1st block	17

Nomenclature

$A^{'}$: Feed spacer characteristic (-)

A_m : Effective membrane area (m^2)

$A_{w(T)}$: Water permeability constant at operating temperature (m/s atm)

$A_{ev,i}$: Exchange area of i-th evaporator (m^2)

$A_{ph,i}$: Exchange area of i-th pre-heater (m^2)

A_{cond}: Exchange area of final condenser (m^2)

$A_{ev,mean}$: Mean exchange area of evaporators (m^2)

$A_{ph,mean}$: Mean exchange area of pre-heaters (m^2)

B_i : Brine rejected by the i-th effect (kg/s)

$B_{s(T)}$: Solute transport parameter at operating temperature (m/s)

C_b : Bulk concentration of a single membrane (kg/m^3)

C_f : Feed concentration of a single membrane (kg/m^3)

$C_{f(plant)}$: Plant feed concentration (kg/m^3)

C_p : Permeate concentration at the permeate channel of a single membrane (kg/m^3)

C_r : Retentate concentration of a single membrane (kg/m^3)

C_w : Membrane surface concentration of a single membrane (kg/m^3)

CR: Compression ratio in the steam ejector (-)

D_i: Total distillate produced in i-th effect (kg/s)

D_b : Diffusivity parameter (m^2/s)

d_h : Hydraulic diameter of the feed spacer channel (m)

$D_{boil,i}$: Distillate produced by boiling in i-th evaporator (kg/s)

$D_{flash,i}$: Distillate produced by flashing in i-th flashing box (kg/s)

E_s: Specific energy consumption (kJ/kg)

ERD : Energy recovery device (-)

J_w : Water flux through a single membrane (m/s)

k : Mass transfer coefficient (m/s)

k_{dc} : Constant in Eq. (59) in (-)

L : Membrane length (m)

L_f : Length of filament in the spacer mesh (m)

m_f : Coefficient in Eq. (62)

Mb: Rejected brine flowrate (kg/s)

M_{COND}: Flowrate of steam in the final condenser (kg/s)

Md: Distillate from MED process (kg/s)

Mf: Water intake in the first effect (kg/s)

Mm: Motive steam flowrate (kg/s)

Ms: Total steam flowrate (kg/s)

Mw: Intake water flowrate (kg/s)

M_{TVC}: Vapor flowrate entrained in TVC section (kg/s)

n: Number of effects of MED process (-) and the spacer characteristics in RO process (-)

PFC: Pressure Correction Factor (-)

P_v: Pressure of saturated steam at temperature T_v (kPa)

P_s: Pressure of saturated steam at temperature T_s (kPa)

P_m: Pressure of saturated steam at temperature T_m (kPa)

P_{ev}: Pressure of saturated entrained vapor (kPa)

P_{crit}: Critical pressure of water (kPa)

P_f : Operating feed pressure of a single membrane (atm)

$P_{f(plant)}$: Plant feed pressure (atm)

P_p : Permeate pressure at the permeate channel (atm)

P_r : Retenate pressure of a single membrane (atm)

$P_{r(plant)}$: Plant retenate pressure (atm)

Q_b : Bulk flowrate of a single membrane (m³/s)

Q_f : Feed flowrate of a single membrane (m³/s)

$Q_{f(plant)}$: Plant feed flow rate (m³/s)

Q_p : Total permeate flow rate of a single membrane (m³/s)

$Q_{p(plant)}$: Plant permeate flow rate (m³/s)

$Q_{p(PV)}$: Permeate flow rate of single pressure vessel (m³/s)

Q_r : Retentate flowrate of a single membrane (m³/s)

$Q_{r(plant)}$: Plant retentate flowrate (m³/s)

Q_s : Total solute flux through the membrane (kg/m² s)

Q_{COND}: Thermal load in final condenser (kW)

$Q_{sensible}$: Sensible heat used in first effect (kJ/kg)

Q_{latent}: Latent heat used in first effect (kJ/kg) Q_i:

Thermal load at i-th evaporator (kW)

Q_s: Thermal load of steam (kW)

Ra: Entrainment ratio (-)

Re_b : Reynolds number (-)

Rec : Total recovery rate of a single membrane (-)

$Rec_{(plant)}$: Plant recovery rate (-)

Rej : Total solute rejection (-)

$Rej_{(plant)}$: Plant solute rejection (-)

Sc : Schmidt number (-)

t_i: Feed temperature after i-th pre-heater (°C)

t_f : Height of feed channel of the membrane (m)

tn: Feed temperature after final condenser (°C)

$T1$: Top brine temperature (Ttop) (°C)

Tb: Temperature of rejected brine (°C)

Ts: Steam temperature (°C)

Tv_i: Temperature of the vapor phase in i-th effect (°C)

Tw: Temperature of the cooling water (°C)

T_{mean}: Mean temperature in the plant (°C)

T_{crit}: Critical temperature of water (°C)

TCF: Temperature Correction Factor (-)

$U_{ev,i}$: Global heat exchange coefficient in i-th evaporator (kW/m^2 °C)

$U_{ph,i}$: Global heat exchange coefficient in i-th pre-heater (kW/m^2 °C)

U_{cond}: Global heat exchange coefficient in final condenser (kW/m^2 °C)

U_b : Cross flow velocity of a single membrane (m/s)

W : Membrane width (m)

x_i: Salinity in i-th evaporator (ppm or w/w%)

xb: Salinity in rejected brine (ppm or w/w%)

xf: Salinity in the feed (ppm or w/w%)

x_{mean}: Mean salinity in the plant (ppm or w/w%)

Greek

α: Fraction of rejected brine from previous effect flashed in the associated pre-heater (-)

β: Fraction of total distillate boiled in each evaporator (-)

$\Delta A_{ev}\%$: Percentage error on evaporators' areas (%)

$\Delta A_{ph}\%$: Percentage error on pre-heaters areas (%)

$\Delta T_{ex,i}$: Driving force for heat exchange in i-th evaporator (°C)

$\Delta t_{\log,i}$: Driving force for heat exchange in i-th pre-heater (°C)

$\Delta T_{\log,cond}$: Driving force for heat exchange in final condenser (°C)

ΔT_i : Temperature drop between two evaporators (°C)

Δt_i : Temperature increase between two pre-heaters (°C)

$\Delta P_{drop,E}$: Total pressure drop along the membrane element (atm)

λ: Latent heat of evaporation (kJ/kg)

π_p : Total osmotic pressure at the permeate channel (atm)

π_w : Total osmotic pressure at the membrane surface (atm)

ρ_b : Density parameter (kg/m^3)

μ_b : Kinematic viscosity (kg/m s)

ε : Membrane porosity (-)

References

Abbas A., 2005. Simulation and anlysis of an industrial water desalination plant. *Chemical Engineering and Processing*, 44, 999–1004.

Abid H.S., Johnson D.J., Hashaikeh R., Hilal N., 2017. A review of efforts to reduce membrane fouling by control of feed spacer characteristics. *Desalination*, 420, 384-402.

Al-Obaidi M.A., Li J-P., Kara-Zaïtri C., Mujtaba I.M.., 2017a. Optimisation of reverse osmosis based wastewater treatment system for the removal of chlorophenol using genetic algorithms. *Chemical Engineering Journal*, 316, 91–100.

Al-Obaidi M.A., Kara-Zaïtri C., Mujtaba I.M., 2017b. Development of a mathematical model for apple juice compounds rejection in a spiral-wound reverse osmosis process. *Journal of Food Engineering*, 192, 111–121.

Al-Sahali M, Ettouney H., 2007. Developments in thermal desalination processes: design, energy, and costing aspects. *Desalination*, 214, 227–240.

Altaee A., Hilal N., 2015. High recovery rate NF–FO–RO hybrid system for inland brackish water treatment. *Desalination*, 363, 19–25.

Ang W.L., Nordin D., Mohammad A.W., Benamor A., Hilal N., 2017. Effect of membrane performance including fouling on cost optimization in brackish water desalination process. *Chemical Engineering Research and Design*, 117, 401–413.

Cardona E., Piacentino A., Marchese F., 2007. Performance evaluation of CHP hybrid seawater desalination plants. *Desalination*, 205, 1–14.

Da Costa A.R., Fane A.G., Wiley D.E. 1994. Spacer characterization and pressure drop modelling in spacer-filled channels for ultrafiltration. *J. Membr. Sci*., 87, 79–98.

Darwish M., Al-Juwayhel F., Abdulraheim H.K., 2006. Multi-effect boiling systems from an energy viewpoint, *Desalination* 194, 22–39.

Edition F. Guidelines for drinking-water quality. WHO Chron, 2011,38(4),104–108.

El-Dessouky HT, Ettouney H.M, Alatiqi I., Bingulac M., 1998. Steady-state analysis of the Multiple effect evaporation desalination process. *Chemical Engineering and Technology*, 21, 437–471

El-Dessouky HT, Ettouney H.M., 2002. *Fundamentals of salt water desalination*. Elsevier.

El-Sayed Y.M., Spiegler K.S., 2001. The energetics of desalination processes. *Desalination*, 134, 109–128.

Gude V.G., Nirmalakhandan N., Deng S., 2010. Renewable and sustainable approaches for desalination. *Renewable and Sustainable Energy Reviews*, 14, 2641-2654.

Process System Enterprise Ltd. 2001. gPROMS Introductory User Guide. London: Process System Enterprise Ltd.

Helal A., 2009. Hybridization - a new trend in desalination. *Desalination and Water Treatment*, 3, 120-135.

Helal A, El-Nashar A, Al-Katheeri E, Al-Malek S., 2004. Optimal design of hybrid RO/MSF desalination plants Part II: Results and discussion. *Desalination*, 160, 13-27.

Hamed O.A., 2005. Overview of hybrid desalination systems — current status and future prospects. *Desalination*, 186, 207–214.

Karan H. Mistry , Mohamed A. Antar, John H. Lienhard V, 2012. An improved model for multiple effect distillation. *Desalination* 51, 807–821.

Koroneos C., Dompros A., Roumbas G., 2007. Renewable energy driven desalination systems modelling. *J. Clean. Prod.*, 15, 449–464.

Lonsdale H.K., Merten U., Riley R.L., 1965. Transport properties of cellulose acetate osmotic membranes. *J. Appl. Polym. Sci.*, 9, 1341–1362.

Mahbub F., Hawlader M.N.A., Mujumdar A.S., 2009. Combined water and power plant (CWPP) — a novel desalination technology. *Desalination and Water Treatment*, 5, 172-177.

Manesh M.H.K., Ghalami H., Amidpour M., Hamedi M.H., 2013. Optimal coupling of site utility steam network with MED-RO desalination through total site analysis and exergoeconomic optimization. *Desalination*, 316, 42–52.

Olwig R, Hirsch T, Sattler C, Glade H, Schmeken L, Will S, et al., 2012. Techno-economic analysis of combined concentrating solar power and desalination plant configurations in Israel and Jordan. *Desalination and Water Treatment*, 41, 9–25.

Ophir A, Lokiec F., 2005. Advanced MED process for most economical sea water desalination. *Desalination*, 182, 187–198.

Rensonnet T., Uche J., Serra L., 2007. Simulation and thermoeconomic analysis of different configurations of gas turbine (GT)-based dual purpose power and desalination plants (DPPDP) and hybrid plants (HP). *Energy*, 32, 1012–1023.

Sadri S., Ameri M., Khoshkhoo R.H., 2017. Multi-objective optimization of MED_TVC-RO hybrid desalination system based on the irreversibility concept. *Desalination*, 402, 97–108.

She Q., Wang R., Fane A.G., Tang C.Y., 2016. Membrane fouling in osmotically driven membrane processes: A review. *J. Membr. Sci.*, 499, 201–233.

Toray, operation, maintenanve and handling manual for membrane elements, 2015. http://www.toraywater.com/knowledge/kno_003.html, (Accessed on 1/4/2018).

Veolia Water, 2011. Fujairah 2 reverse osmosis desalination plant. http://www.veolia.com/middleeast/sites/g/files/dvc171/f/assets/documents/2015/09/Fujairah_2_RO.pdf, (Accessed on 8/5/2018).

Weiner A.M., Blum D.H., Lienhard V J.H., Ghoniem A.F., 2015. Design of a hybrid RO-MED solar desdalination system for training agricultural draining water in california. The International Desalination Association World Congress on Desalination and Water Reuse, San Diego, CA, USA. *Desalination*; 182 ,187–198.